Magnetoresistive studies on nanocrystalline $La_{0.8}Sr_{0.2}MnO_{3+\delta}$ manganite

B.M. Nagabhushana [a,**], R.P. Sreekanth Chakradhar [b,*], K.P. Ramesh [c], V. Prasad [b], C. Shivakumara [d], G.T. Chandrappa [e]

[a] Department of Chemistry, M.S. Ramaiah Institute of Technology, Bangalore 560 054, India
[b] Glass Technology Laboratory, Central Glass and Ceramic Research Institute, Council of Scientific and Industrial Research (CSIR), Kolkata 700032, India
[c] Department of Physics, Indian Institute of Science, Bangalore 560 012, India
[d] Solid State and Structural Chemistry Unit, Indian Institute of Science, Bangalore 560 012, India
[e] Department of Chemistry, Central College Campus, Bangalore University, Bangalore 560 001, India

ARTICLE INFO

ABSTRACT

Low-temperature magnetoresistance (MR) measurement has been carried out on nanocrystalline $La_{0.8}Sr_{0.2}MnO_{3+\delta}$ manganites prepared by combustion synthesis. This preparation method yields voluminous powders with large surface area ($\sim$40 m^2/g) having crystalline nanosize ($\sim$50 nm) products. Formation and homogeneity of the solid solutions have been confirmed by powder X-ray diffraction (PXRD), scanning electron microscopy (SEM) and energy-dispersive spectroscopy (EDS). Rietveld refinement of X-ray data indicates that as-formed compound exhibits cubic phase with space group Pm3 m. However, calcined sample transforms into rhombohedral phase with space group R-3c. The stabilization of the cubic phase in as-formed manganite is due to the substitution of Sr^{2+} on La^{3+} sites, resulting in higher Mn^{4+} content. The low-temperature resistivity measurements down to 70 K exhibit a broad metal–insulator transition (T_{M-I}) at around 257 K. MR measurements on sintered pellets show $\sim$5% MR at 1 T, whereas for 4 and 7 T, the %MR values are found as 22% and 28%, respectively, at T_{M-I}.

© 2008 Elsevier B.V. All rights reserved.

1. Introduction

In recent years, nanotechnology has emerged as an attractive field for the development of novel materials having unusual properties and has provided different pathways to solve many unresolved issues in various fields including colossal magnetoresistance (CMR) material. The results of earlier investigations [1] show that the properties of nanocrystalline manganites can essentially change with decreasing particle size. Perovskite-type strontium-doped lanthanum manganites, $La_{1-x}Sr_xMnO_{3+\delta}$, is of interest for a number of possible applications due to its unique physical and chemical properties such as catalysis [2–4], giant magnetoresistance (GMR) and possibly for use as an electrode materials for solid-oxide fuel cell [5–7]. Use of materials belonging to this category depends not only on their chemical, structural and thermodynamic characteristics but also on their final microstructure, grain size and pore size distribution. These characteristics depend on the processing conditions but are hardly controllable in the conventional ceramic synthesis process based on the diffusion of the components in the solid state at high temperature.

Various techniques including the combustion process are available for the preparation of nanocrystalline manganites. They comprise of dividing (breaking down a bulk solid) or building up processes. Some of the well-known methods are sol–gel [8], co-precipitation [9] and hydrothermal [10]. All these techniques require special chemicals and equipments and have various disadvantages. However, the low-temperature-initiated solution combustion process is an attractive synthetic route for the preparation of multi-component oxide materials, developed by Patil et al. [11–13]. This method, in fact, makes possible the rapid synthesis of several refractory inorganic materials and advanced ceramics, without the prolonged high-temperature treatment of sintering. Solution combustion process is instantaneous, fast, requiring the least external energy input. The reactants are mixed in atomic/molecular levels, so that the final products are obviously more homogeneous. The products are nanocrystalline with large surface area than those prepared by the conventional solid-state method [14]. Phase purity and homogeneity are achieved at low temperature as low as 300 °C as against 1300 °C needed to synthesize these manganites using the solid-state method. The combustion-derived $La_{1-x}Sr_xMnO_{3+\delta}$

** Also corresponding author.
* Corresponding author. Tel.: +91 33 2473 3469x3324; fax: +91 33 2483 8085.
E-mail addresses: chakra@cgcri.res.in, q3c5@yahoo.com
(R.P. Sreekanth Chakradhar).

($x = 0.2$) sample has high Mn^{4+} content, and hence it exhibits cubic phase and rhombohedral phase upon calcination. These phases are favorable for ferromagnetic and metal–insulator property in manganites.

In the present work, we have prepared $La_{0.8}Sr_{0.2}MnO_{3+\delta}$ nanocrystalline manganites through the solution combustion method and the samples are characterized by powder X-ray diffraction (PXRD), SEM, FTIR, TG-DTA and surface area analysis. The magnetoresistance (MR) measurements were performed on sintered (900 °C, 6 h) pellets using the four-probe method from 300 down to 70 K. In order to understand the conduction mechanism especially in ferromagnetic low-temperature regime, an attempt is made to fit the resistivity data with simple empirical equation.

2. Experimental

2.1. Synthesis of $La_{0.8}Sr_{0.2}MnO_{3+\delta}$

In a typical synthesis, the stoichiometric amounts of combustible redox mixture containing metal nitrates (oxidizers) and a fuel (reducer) are subjected for combustion reaction at much low temperature ($\sim$300 °C) in a preheated furnace, and the detailed procedure is given elsewhere [15,16]. In the actual preparation of $La_{0.8}Sr_{0.2}MnO_{3+\delta}$, the stoichiometric quantities high-purity lanthanum, manganese and strontium nitrates and ODH [17] were mixed in a minimum quantity of double distilled water. The solution mixture is concentrated by heating it in a Petri dish on a hot plate until excess free water evaporated and wet product is obtained. Then the Petri dish is introduced into a muffle furnace maintained at 300 ± 10 °C. This precursor mixture of water, metal nitrates and fuel decomposes and ruptures into a flame within about 3–5 min. The resultant product is a voluminous, foamy powder, which occupies the entire volume of the reaction vessel.

3. Results and discussion

3.1. Structural and micro-structural characterization

The phase purity and crystal structure were examined by the Philips X-ray diffractometer using Cu K$_\alpha$ radiation with a nickel filter. Fig. 1 shows PXRD patterns of as-formed and calcined (900 °C, 6 h) $La_{0.8}Sr_{0.2}MnO_{3+\delta}$ samples. The as-formed $La_{0.8}Sr_{0.2}MnO_3$ sample shows crystalline cubic symmetry with space group $Pm3\,m$, besides extra peaks corresponding to $SrCO_3$ impurity. However, calcined (900 °C for 6 h) sample exhibit rhombohedral phase with space group R-$3c$ (hexagonal setting). In the calcined sample, the diffraction peaks are narrower and slightly shifted to lower 2θ values, indicating an increase in the particle size and the substitution of strontium for lanthanum. The structural parameters of calcined $La_{0.8}Sr_{0.2}MnO_{3+\delta}$ sample evaluated by standard Rietveld technique are found to be $a = 5.462(3)$Å, and $c = 13.4361$ Å, with a unit cell volume of $V = 57.86\ (3)(\text{Å})^3$. The existence of strong oxidizing atmosphere at elevated temperature during combustion reaction leads to excess formation of $Mn^{4+}(>38\%)$ in as-formed $La_{0.8}Sr_{0.2}MnO_{3+\delta}$ sample stabilizing the cubic phase. It can be seen from the PXRD patterns that they are quite broad, indicating the nanocrystalline nature. The crystallite size of as-formed and calcined powders were calculated from the width of the X-ray diffraction peaks using Scherrer's formula [18] and found to be in the range 30 and 50 nm, respectively. It is clear from Fig. 1, upon calcinations the full width at half maxima (FWHM) of (110) diffraction peak decreases, which confirms the increase in crystallite size upon
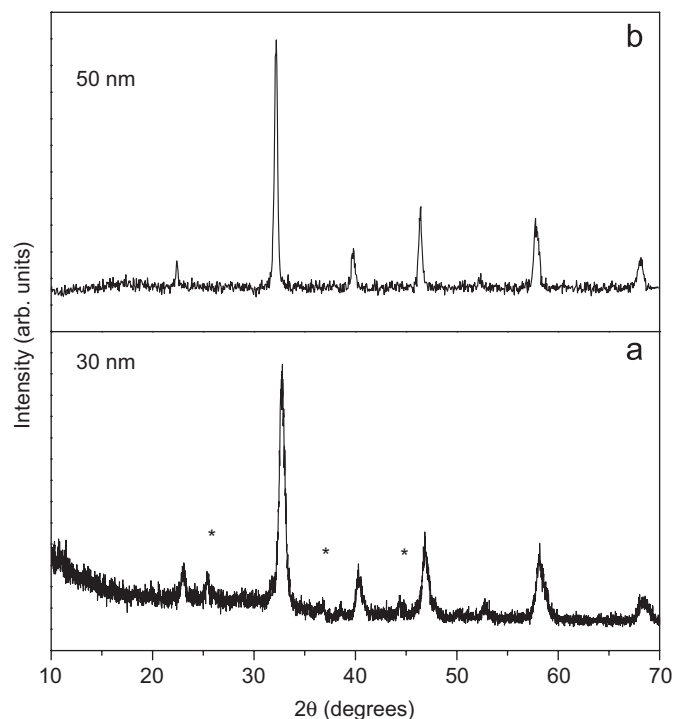

Fig. 1. PXRD patterns of (a) as-formed and (b) calcined (900 °C, 6 h) $La_{0.8}Sr_{0.2}MnO_{3+\delta}$ samples (*$SrCO_3$ impurity peaks).

calcination. The FWHM for as-formed sample is 0.580°, whereas for calcined sample it is $\sim$0.373°.

The surface morphology of the products was examined by JEOL (JSM-840 A) scanning electron microscopy (SEM). The morphology of the powders before and after calcination is shown in Fig. 2. The SEM micrograph of combustion-derived sample shows (Fig. 2a) that the product is voluminous and porous as a result of large amount of gases evolved during the combustion reaction. The micrograph of as-formed powder has irregular shaped agglomerates with cage-like structure. After calcinations (Fig. 2b) the size of primary particle increases, which leads to decrease in surface area of the sample as expected which is confirmed by surface area measurements. The surface areas of the as-formed and calcined $La_{0.8}Sr_{0.2}MnO_{3+\delta}$ samples were determined by the BET method using nitrogen as adsorbent gas [19]. The combustion-derived products usually exhibit good surface area, because the heat generated (exothermicity) during combustion reaction would be long enough to form nucleus but too short for grain growth. As-formed $La_{0.8}Sr_{0.2}MnO_{3+\delta}$ powder has surface area of about 40.7 m^2/g, whereas the calcined (900 °C, 6 h) sample shows 28.2 m^2/g, the reduction in surface area is attributed due to the congregation effect.

The energy-dispersive spectroscopy (EDS) analysis confirmed the composition and homogeneous distribution of the constituent elements. The average composition for $La_{0.8}Sr_{0.2}MnO_{3+\delta}$ obtained from EDS spectra recorded at different areas and the values are agreeing well in terms of atomic ratio (La: Sr: Mn = 0.79: 0.19: 1.01) with the starting composition (La: Sr: Mn = 0.8: 0.2: 1.0)

The Mn^{4+} content is a crucial factor in determining the magnetic and transport properties of hole doped manganites. Mixed valence states of Mn (Mn^{3+}/Mn^{4+}) is essential for both metallic and ferromagnetic behaviors in doped manganites [20–22]. The Mn^{4+} content in combustion-derived $La_{0.8}Sr_{0.2}MnO_{3+\delta}$ samples prepared in this investigation was estimated from the iodometric titration [23], and it is found to lie in the
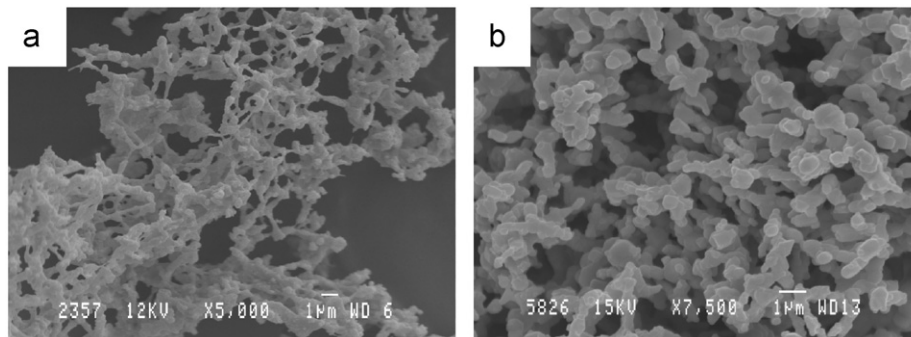
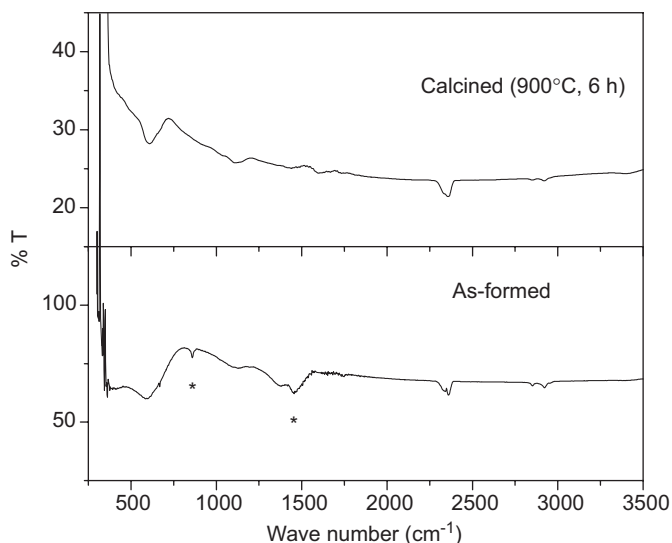**Fig. 2.** SEM micrographs of (a) as-formed and (b) calcined (900 °C, 6 h) $La_{0.8}Sr_{0.2}MnO_{3+\delta}$ samples.

Fig. 3. FTIR spectra of series of as-formed and calcined $La_{0.8}Sr_{0.2}MnO_{3+\delta}$ samples (*$SrCO_3$).

range between $42\pm4\%$ and $38\pm4\%$ for as-formed and calcined $La_{0.8}Sr_{0.2}MnO_{3+\delta}$ samples, respectively. It is observed that combustion derived samples show higher percentage of Mn^{4+} content compared to the samples prepared via the ceramic route [14].

Thermal analysis (TG-DTA) of as-formed $La_{0.8}Sr_{0.2}MnO_{3+\delta}$ was carried out at the rate of 10 °C/min from room temperature to 1300 °C, no endothermic peak is observed in the DTA curve, which indicates that there is no dehydration or phase change of the precursors or the products. A broad exothermic peak was observed around 900 °C in the DTA curve, which corresponds to the reduction of Mn^{4+} to Mn^{3+} state. The TG result shows a weight loss around 600 °C and this gradual weight loss is continued due to the reduction of Mn^{4+} to Mn^{3+} with increase in temperature.

Fig. 3 shows the FTIR spectra of as-formed and calcined (900 °C, 6 h) $La_{0.8}Sr_{0.2}MnO_{3+\delta}$ samples. The band around $600\,cm^{-1}$ corresponds to the stretching mode v_s, which involves the internal motion of a change in Mn−O−Mn bond length; the band around $400\,cm^{-1}$ corresponds to the bending mode v_b, which is sensitive to a change in Mn−O−Mn bond angle. In as-formed sample, other two absorption bands at 860 and $1450\,cm^{-1}$ were observed corresponding to $SrCO_3$ impurity peaks which disappeared on calcination. These results are also supported by PXRD analysis. These two bands are related to the environment surrounding the MnO_6 octahedra. The most interesting feature of the IR spectra presented in Fig. 3 is the diminishing of the intensity of Mn−O−Mn bending mode v_b upon calcination.

3.2. Transport and magnetic properties

The combustion-derived nanodimensional manganite sample shows different resistivity behavior from those reported in single crystals [22] as well as the samples prepared by the ceramic route [24]. Perovskite manganites with bigger grain size exhibit sharp metal–insulator transition; however, combustion derived samples show a broad metal–insulator transition due to the nanocrystalline nature of the grains. For instance, in the present study, $La_{0.8}Sr_{0.2}MnO_{3+\delta}$ sample exhibits metal–insulator transition at 257 K at zero field. This value is low compared to the samples prepared by the ceramic route [24]. The metal–insulator transition temperature of polycrystalline manganites significantly depends on grain size. The reduction of grain size leads to a decrease in metal–insulator transition temperature. The effect of particle size on the $T_{M−I}$, magnetization and MR values have also been reported by various investigators [1,25,26].

The transport behavior of the granular perovskite system can be strongly influenced by intrinsic properties in the cores. Two kinds of MR are observed in granular perovskites [26], one is tunnel type of GMR due to interfacial tunneling and the other one intrinsic CMR due to intrinsic transport behavior. According to Zhang et al. [26] the interfaces between neighboring grains are assumed to be the intergranular barriers due to the magnetic disorder in the grain surfaces. An itinerant electron, which comes from the 3d shell e_g^1 orbit of the Mn^{3+} ion, can hop grain to grain through spin-dependent interfacial tunneling. Interfacial tunneling must be a universal phenomenon that exists in granular manganese perovskites.

The MR measurements were performed on sintered (900 °C for 6 h) pellets using the four-probe method using a variable temperature insert (Janis Supervaritemp Cryostat) from 300 down to 70 K and super conducting magnet. Fig. 4 shows the temperature dependence of the resistivity of $La_{0.8}Sr_{0.2}MnO_{3+\delta}$ pellets at different magnetic fields. It can be seen from Fig. 4 that the resistivity decreases with increasing magnetic field and that of $T_{M−I}$ shifts towards higher temperature. The resistivity at $T_{M−I}$ is maximum, above which it decreases with increasing temperature, characteristic similar to semiconductor, while below $T_{M−I}$, the resistance decreases with temperature, like metals. The $T_{M−I}$ of $La_{0.8}Sr_{0.2}MnO_{3+\delta}$ is 257, 262, 267 and 270 K under zero, 1, 4, and 7 T, respectively.

Fig. 5 shows the resistivity behavior of sintered pellet at 0, 1, 4 and 7 T at 85, 257 and 298 K. As applied magnetic field increases the resistivity decreases monotonically. The decrease in resistivity may be due to the fact that the applied magnetic field induces delocalization of charge carriers, which in turn might suppress the resistance and also cause the local ordering of the magnetic spins. Due to this ordering, the ferromagnetic metallic state may suppress the paramagnetic insulating regime. As a result,
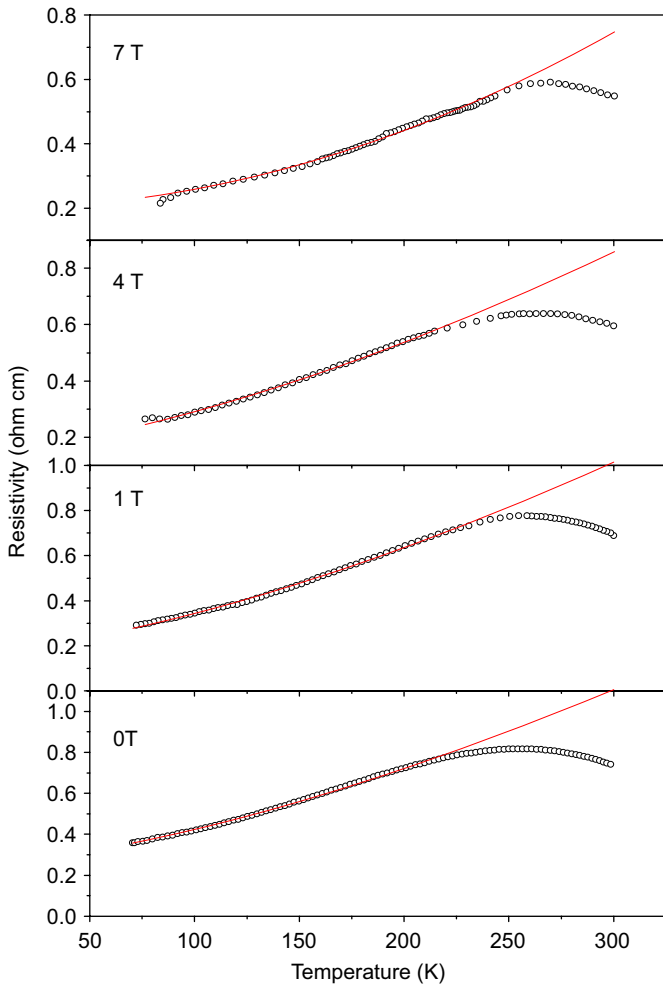
Fig. 4. Resistivity Vs temperature below T_{M-I} both in the absence and presence of magnetic field 1, 4 and 7 T. Solid line gives the best fit to equation $\rho = \rho_1 + \rho_2 T_2$.

Fig. 5. Resistivity Vs applied magnetic field at 85, 257 and 298 K.

conduction electrons (e_g^1) are easily transferred between pairs of Mn^{3+} (t_{2g}^3 e_g^1: $S = 2$) and Mn^{4+} (t_{2g}^3 e_g^0: $S = \frac{3}{2}$) via oxygen and therefore T_{M-I} shifts to higher temperature with application of magnetic filed. In fact, randomly oriented moments of grains can be aligned by an external field. This causes a significant increase in tunnel conductance, thereby reducing resistivity of the granular system.

The percentage change of MR values of samples in the vicinity of T_{M-I} have been calculated using the well-known relation MR % $= 100 \times [\rho(H) - \rho(0)]/\rho(0)$, where $\rho(H)$ and $\rho(0)$ are the resistivities at a given temperature in the presence and absence of a magnetic field (H). The MR values at T_{M-I} for 1, 4 and 7 T correspond to ∼5%, 22% and 28%. Whereas the negative MR values at low temperature (85 K) are found to be 18%, 32% and 40%, respectively, for 1, 4 and 7 T applied magnetic field. The applied magnetic field induces delocalization of charge carriers, which in turn might suppress the resistance and also causes the local ordering of the magnetic spins.

In order to understand the conduction mechanism especially in ferromagnetic low-temperature ($T < T_{M-I}$) regime, an attempt is made to fit the resistivity data below T_{M-I} to the empirical equation:

$$\rho = \rho_1 + \rho_2 T^n$$

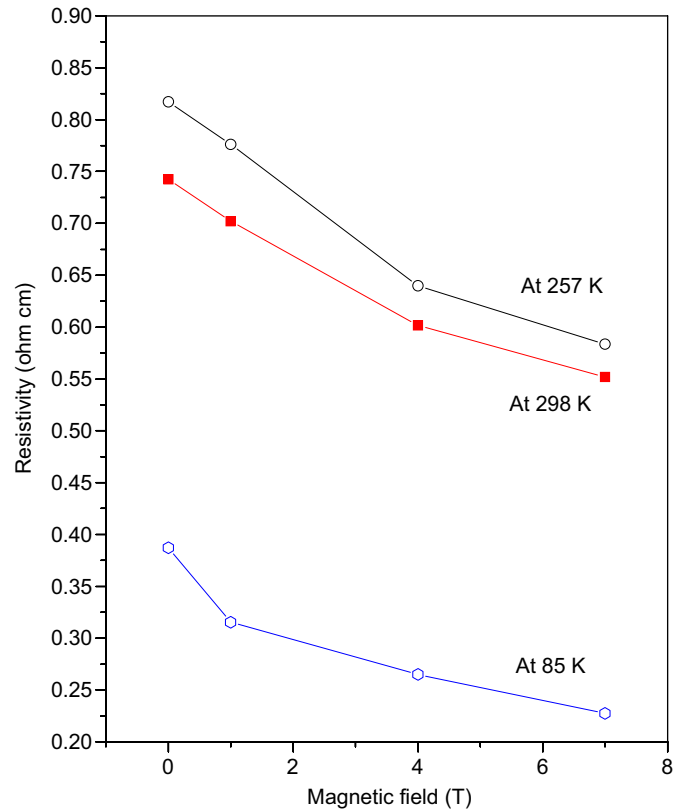where ρ_1 represents the residual resistivity due to the grain boundary effect. The residual resistivity (ρ_1) in nanostructured manganites is more than single crystals or large grain size samples. Jia et al. [27] have discussed the role of the grain boundaries in the manganites. According to the report, the finite MR obtained for polycrystalline manganite materials for $T < T_c$ most likely resulted from grain boundary scattering. It is believed that the difference in resistivity behavior between single crystal and polycrystalline manganites is due to the grain boundary contribution and this is large for polycrystalline manganites. The residual resistivity (ρ_1) in nanostructured manganites is an additive factor and hence the total resistivity (ρ) for nanocrystalline materials is always higher compared to single crystals and large grain size samples.

The experimental data of a material (best fit) can be tested by evaluating a statistical term, known as the square of linear correlation coefficient (R^2). As the value of R^2 in this case is found to be 0.996 and the fitting to the equation yields a value of $n = 2$. The term $\rho_2 T^2$ indicates resistivity due to the electron–electron scattering process in the ferromagnetic phase. It has been concluded that the variation of electrical resistivity data fits very well with this equation. The above fit shows that the double exchange interaction plays a major role on the MR behavior of the sample. The solid lines in Fig. 4 represent the fit. Further, the parameter ρ_1 is found to decrease (0.260, 0.1833, 0.1556 and 0.1978 ohm cm, respectively, for 0, 1, 4 and 7 T) as magnetic field increases and this may be due to the enlargement of magnetic domains.

4. Conclusions

Nanocrystalline single-phase La$_{0.8}$Sr$_{0.2}$MnO$_{3+\delta}$ powder has been prepared by combustion route at much lower temperature. The synthesis temperature employed is lower than those currently used in the conventional route and also the time taken

for preparation is only a few minutes. This method yields a homogeneous and good surface area nanocrystalline powders. We observed a metal–insulator transition around 257 K. $La_{0.8}Sr_{0.2}MnO_{3+\delta}$ sample exhibits field-induced ferromagnetic ordering and shows a negative magnetoresistance. The low-temperature metallic resistivity data are fitted to the double exchange model.

Acknowledgments

References

[1] N. Zhang, W. Ding, W. Zhong, W. Yang, Y. Du, J. Phys.: C. Matter 9 (1996) 4281.
[2] W.F. Libby, Science 171 (1971) 449.
[3] P.K. Gallagher, D.W. Johnson Jr., F. Schrey, Mater. Res. Bull. 9 (1974) 1345.
[4] R.J.H. Voorhoeve, D.W. Johnson Jr., J.P. Remeika, P.K. Gallagher, Science 195 (1977) 827.
[5] H. Taimatsu, K. Wada, H. Kaneko, J. Am. Ceram. Soc. 75 (1992) 401.
[6] L. Kindermann, D. Das, H. Nickel, K. Hilpert, J. Electrochem. Soc. 144 (1997) 717.
[7] P.J. Gellings, H.J.M. Bouwmeester (Eds.), The CRC Handbook Solid State Electrochemistry, CRC Press, New York, 1997, p. 407.
[8] QI-Hui Wu, Meilin Liu, W. Jaegermann, Mater. Lett. 59 (2005) 1980.
[9] A. Ghosh, A.K. Sahu, A.K. Gulnar, A.K. Suri, Scripta Materallia 52 (2005) 1305.
[10] Jeroen Spooren, Richard I. Walton, Franck Millange, J. Mater. Chem. 15 (2005) 1542.
[11] R. Gopi Chandran, K.C. Patil, G.T. Chandrappa, J. Mater. Sci. 31 (1996) 5773.
[12] J.J. Kingsley, K.C. Patil, Mater. Lett. 6 (1988) 427.
[13] K.C. Patil, S.T. Aruna, Ekambaram, Curr. Opinion Solid State Mater. Sci. 2 (1997) 158.
[14] R. Mahesh, R. Mahendrian, A.K. Raychudhuri, C.N.R. Rao, J. Solid State Chem. 114 (1995) 297.
[15] R.P. Sreekanth Chakradhar, B.M. Nagabhushana, G.T. Chandrappa, K.P. Ramesh, J.L. Rao, J. Chem. Phys. 121 (2004) 10250.
[16] R.P. Sreekanth Chakradhar, B.M. Nagabhushana, G.T. Chandrappa, K.P. Ramesh, J.L. Rao, Mater. Chem. Phys. 95 (2006) 169.
[17] G. Gran, Anal. Chim. Acta. 14 (1956) 150.
[18] H. Klug, L. Alexander, X-ray Diffraction Procedures, Wiley, New York, 1962, p. 491.
[19] S. Brunauer, P.H. Emmett, E. Teller, J. Am. Chem. Soc. 66 (1938) 309.
[20] G.H. Jonker, J.H. Van Santen, Physica 16 (1950) 337.
[21] C. Zener, Phys. Rev. 82 (1951) 403.
[22] H.Y. Hwang, S.W. Cheong, N.P. Ong, B. Balogg, Phys. Rev. Lett. 77 (1996) 2041.
[23] R.N. Singh, C. Shivakumara, N.Y. Vasanthacharya, S. Subramanian, M.S. Hegde, H. Rajagopal, A. Sequeria, J. Solid State Chem. 132 (1998) 19.
[24] R. Mahendiran, A.K. Rayachaudhuri, A. Chainani, D.D. Sarma, S.B. Roy, Appl. Phys. Lett. 66 (1995) 233.
[25] R.D. Sanchez, J. Rivas, C. Va′zquez-Vazquez, A. Lopez- Quintela, M.T. Causa, M. Tovar, S. Oseroff, Appl. Phys. Lett. 68 (1996) 134.
[26] N. Zhang, W. Ding, W. Zhong, D. Xing, Y. Du, Phys. Rev. B 56 (1997) 8138.
[27] Y.X. Jia, Lu, Li, K. Khazeni, V.H. Crespi, A. Zettl, M.L. Choen, Phy. Rev. B 52 (1995) 9147.